Fluorophore-Assisted Light Inactivation of Calmodulin Involves Singlet-Oxygen Mediated Cross-Linking and Methionine Oxidation†

Ping Yan, Yijia Xiong, Baowei Chen, Sewite Negash, Thomas C. Squier, and M. Uljana Mayer*

Cell Biology and Biochemistry Group, Division of Biological Sciences, Pacific Northwest National Laboratory, Richland, Washington 99352

Received November 22, 2005; Revised Manuscript Received February 16, 2006

ABSTRACT: Fluorophore-assisted light inactivation (FALI) permits the targeted inactivation of tagged proteins and, when used with cell-permeable multiuse affinity probes (MAPs), offers important advantages in identifying physiological function, because targeted protein inactivation is possible with spatial and temporal control. However, reliable applications of FALI, also known as chromophore-assisted light inactivation (CALI) with fluorescein derivatives, have been limited by lack of mechanistic information regarding target protein sensitivity. To permit the rational inactivation of targeted proteins, we have identified the oxidizing species and the susceptibility of specific amino acids to modification using the calcium regulatory protein calmodulin (CaM) that, like many essential proteins, regulates signal transduction through the reversible association with a large number of target proteins. Following the covalent and rigid attachment of 4′,5′-bis(1,3,2-dithioarsolan-2-yl)fluorescein (FlAsH) to helix A, we have identified light-dependent oxidative modifications of endogenous methionines to their corresponding methionine sulfoxides. Initial rates of methionine oxidation correlate with surface accessibility and are insensitive to the distance between the bound fluorophore and individual methionines, which vary between ∼7 and 40 Å. In addition, we observed a loss of histidines, as well as zero-length cross-linking with binding partners corresponding to the CaM-binding sites of smooth myosin light chain kinase and ryanodine receptor. Our results provide a rationale for proteomic screens using FALI to inhibit the function of many signaling proteins, which, like CaM, commonly present methionines at binding interfaces.

The availability of annotated and high-quality genomic information, in conjunction with gene array and global proteomic measurements of protein abundances, provides an opportunity to gain a predictive understanding of cell function (*1*−*4*). To accomplish this, efficient methods are needed to rapidly identify the functions of expressed proteins and their linkage to metabolic and signaling pathways. Fluorophore-assisted light inactivation (FALI)[1] with cell-permeable multiuse affinity probes (MAPs) can permit the targeted inactivation of tagged proteins following protein synthesis and localization. FALI offers important advantages in identifying physiological function, because the targeted protein inactivation of intracellular signaling proteins is possible in a way that minimizes adaptive cellular responses commonly observed using gene ablation or silencing methods (*5*). Initial measurements involving light inactivation (CALI) of expressed proteins in cells were pioneered by Jay and coworkers using the chromophore malachite green attached to antibodies against either a surface-exposed protein using a cell model or purified proteins (i.e., alkaline phosphatase or β-galactosidase) (*6*). Subsequent measurements have demonstrated an ability to photoinactivate tagged proteins using fluorescein, green fluorescent protein, and the cell-permeable multiuse affinity probes (MAPs) 4′,5′-bis(1,3,2-dithoarsolan-2-yl)fluorescein (FlAsH-EDT_2) and 4,5-bis(1,3,2-dithiarsolan-2-yl)resorufin (ReAsH-EDT_2), which require lower light levels to induce photoinactivation (*5*, *7*−*9*). However, the applicability of these methods has been limited to selected proteins, and photoinactivation cannot be accomplished in a predictable or reliable manner due to the lack of a molecular mechanism (*10*, *11*).

Current measurements suggest that the photoinactivation of malachite green generates a highly reactive species that can inactivate proteins within a 15−60 Å radius (*11*, *12*). The reactive species generated following illumination of malachite green has been suggested to involve the highly reactive hydroxyl radical, which in aqueous solution essentially reacts at the site of generation (*13*). In contrast, the

† This research was supported by the Genomics: Genomes to Life program of the U.S. Department of Energy's Office of Biological and Environmental Research. Pacific Northwest National Laboratory is operated for the DOE by Battelle Memorial Institute under Contract DE-AC05-76RLO 1830.

* Address correspondence to M. Uljana Mayer, Cell Biology and Biochemistry Group, Pacific Northwest National Laboratory, P.O. Box 999; P7-56, Richland, WA 99352; phone, (509) 376-1681; fax, (509) 376-6767; e-mail: Uljana.Mayer@pnl.gov.

[1] Abbreviations: BME, β-mercaptoethanol; CALI, chromophore-assisted light inactivation; CaM, calmodulin; C4-CaM, calmodulin in which positions 6, 7, 10, and 11 have been mutated to cysteine; EDT, ethanedithiol; EGTA, ethylene glycol bis(2-aminoethyl ether)-*N*,*N*,*N*′,*N*′-tetraacetic acid; FALI, fluorophore-assisted light inactivation; FCS, fluorescence correlation spectroscopy; FlAsH-EDT_2, 4′,5′-bis(1,3,2-dithioarsolan-2-yl)fluorescein also known as fluorescein arsenical helix binder; HEPES, *N*-(2-hydroxyethyl)piperazine-*N*′-(2-ethanesulfonic acid); LC, liquid chromatography; MALDI, matrix-assisted laser desorption ionization; MAP, multiuse affinity probe; ReAsH-EDT_2, 4,5-bis(1,3,2-dithioarsolan-2-yl)resorufin; RyR, ryanodine receptor; SDS−PAGE, sodium dodecyl sulfate−polyacrylamide gel electrophoresis; TCEP, tris-(carboxyethyl)phosphine.

10.1021/bi052395a CCC: $33.50
Published on Web 03/24/2006

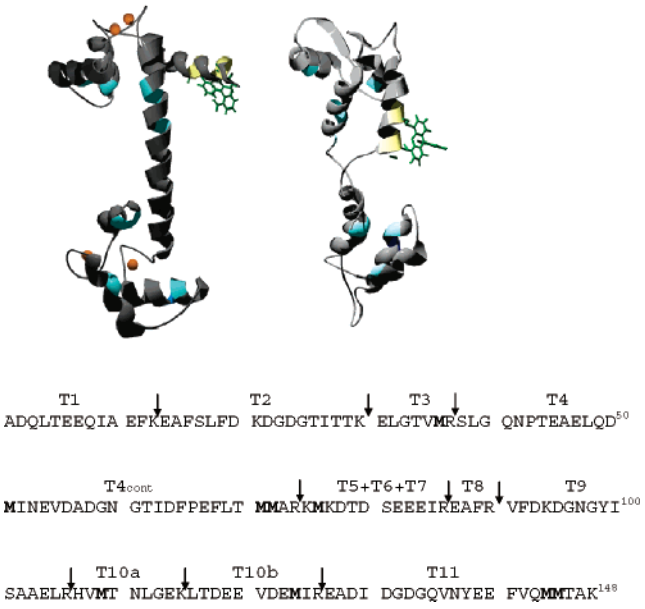

FIGURE 1: Tertiary structures (top) and primary sequence (bottom) for apo-CaM (1cfd.pdb; right) and calcium-saturated CaM (1cll.pdb; left), where calcium ions are depicted as orange spheres. Bound FlAsH (green) is shown on the tertiary structure, and corresponding attachment sites, which involve site-directed substitutions of Glu^6, Glu^7, Ala^{10}, and Glu^{11} with cysteines, are highlighted in yellow. Methionines and histidines in the protein sequence are denoted in light and dark blue, respectively. Positions of trypsin cleavage within the primary sequence are depicted with arrows.

illumination of fluorescein or ReAsH is thought to primarily result in the generation of singlet oxygen ($^1O_2$) (*5*, *7*). However, in no case has the mechanism of protein inactivation been identified, preventing reliable FALI of proteins of interest that should be possible using MAPs or antibodies to target intracellular proteins. We have therefore investigated the mechanism of photoinactivation using the signaling protein calmodulin (CaM), which has previously been tagged and labeled with MAPs with full retention of function as indicated by the unchanged apparent affinity and maximum extent of enzyme activation in a phosphodiesterase binding and activity assay (*14*), as well as labeled with MAPs in living cells (*15*). This protein is a good candidate, because it modulates the function of more than 50 target proteins through reversible binding (*16*). In addition, prior genetic approaches aimed at understanding its specific function in a given pathway have not been successful because of CaM's essential nature. Furthermore, structures are known both in the free and metal-bound forms (Figure 1), and in complex with the CaM-binding sequences of some target proteins that include smooth myosin light chain kinase (MLCK) and the plasma membrane Ca-ATPase (*17*−*23*), permitting a detailed chemical understanding of how light-induced modifications affect function.

Therefore, in this study, we have demonstrated the functional sensitivity of CaM to light-induced inactivation following the covalent binding of FlAsH to helix A near the N-terminus through the same four cysteines genetically substituted into the native sequence that have previously been used for in vivo labeling of CaM (*14*, *15*). Upon light exposure, there is a light-dependent oxidative modification of CaM that requires molecular oxygen and is prevented by inclusion of $^1O_2$ quenchers. HPLC and mass spectrometry were used to identify oxidative modifications following tryptic digestion. We found that there is selective oxidation of endogenous methionines to their corresponding methionine sulfoxides, which diminishes the binding affinity between CaM and the vast majority of target proteins associated with signaling. Initial rates of methionine oxidation correlate with surface accessibility and are insensitive to the distance between the bound fluorophore and individual methionines, which varies between ~7 and 40 Å. These results indicate that the diffusion of $^1O_2$ is sufficient to generate a near-uniform concentration that essentially blankets the protein, where the susceptibility of individual methionines to oxidative modification represents a slow reaction that is determined by relative differences in surface accessibility. In addition, we observed a loss of histidines, which may be responsible for cross-linking with binding partners corresponding to the CaM-binding sites of smooth MLCK and ryanodine receptor (RyR). Contrary to prior reports using model systems with individual amino acids, no other amino acids in CaM are sensitive to modification. Our results, indicating an ability to selectively target methionines for oxidative modification, provide a rationale to selectively target the functions of key signaling proteins, because, like CaM, they commonly present methionines at binding interfaces to facilitate the reversible binding of protein domains. In conclusion, these results provide a solid grounding for the sequence-based choice of proteins for light inactivation as a means for optimal spatial and temporal resolution in cell function measurements.

EXPERIMENTAL PROCEDURES

Materials. Sepharose 4B, Triton X-100, buffers, and other chemical reagents were obtained from Sigma-Aldrich (St. Louis, MO), unless otherwise specified. Sequencing-grade modified trypsin was obtained from Promega (Madison, WI). Oxyrase was purchased from Oxyrase, Inc. (Mansfield, OH). CaM-Sepharose 4B was purchased from Amersham Bioscience (Piscataway, NJ). Complete EDTA-free protease inhibitor cocktail tablets (catalog no. 1 836 170) were obtained from Roche (Indianapolis, IN). Mouse brains were purchased from Pel Freez Biologicals (Rogers, AR). Peptides (>95% purity) corresponding to the CaM-binding sequences of rabbit smooth myosin light chain kinase (RRKWQKTGHAVRAIGRLSSS; MLCK) (*24*), the plasma membrane Ca-ATPase (C28W) (LRRGQILWFRGLNRIQTQIRVVNAFRSS) (*25*), and the ryanodine receptor (KSKKAVWHKLLSKQRRRAVVACFRMTPLYN) (*26*) were synthesized by SynPep (Dublin, CA). The CaM-binding sequence of human smooth muscle myosin kinase (ec 2.7.1.117; RRKWQKTGNAVRAIGRLSSM; MLCK*) was synthesized by Biopeptide Co. (San Diego, CA). 4′,5′-(1,3,2-Dithioarsolan-2-yl)fluorescein (FlAsH-EDT_2) was synthesized as previously described (*15*).

Mutagenesis, Expression, and Purification of the Tetracysteine-CaM Mutant. The gene for CaM, with the four native amino acids at positions 6, 7, 10, and 11 mutated to cysteine, was cloned into a pET-15b plasmid expression vector and expressed in BL21(DE3) *Escherichia coli* cells, as previously described (*14*). Following expression, the tetracysteine-tagged CaM (C4-CaM) was purified by chromatography on phenyl-Sepharose CL-4B (Pharmacia, Piscataway, NJ), essentially as previously described (*27*, *28*)

with the exception of the addition of 5 mM β-mercaptoethanol (BME) to all buffers to prevent oligomerization of C4-CaM. The protein concentration was determined using the micro Bradford protein assay (Bio-Rad 500-0006).

FlAsH Labeling of Tetracysteine-CaM (C4-CaM). Tetracysteine-CaM (60 μM) was incubated with 1.0 mM TCEP in buffer A [20 mM HEPES (pH 7.6), 150 mM NaCl, and 5 mM BME] with 1.0 mM $CaCl_2$ or 1.0 mM EGTA for 30 min at room temperature before addition of 1.1 equiv of FlAsH (1 mM stock in DMSO). The mixture was then incubated at 4 °C for 12 h. To remove unbound FlAsH, the mixture was dialyzed into buffer A at 4 °C in the dark. Under these conditions, CaM is labeled with FlAsH at a stoichiometry greater than 0.9 bound FlAsH per CaM, as determined by integrating peak areas following HPLC separation of the labeled protein. For peptide cross-linking experiments, 1 equiv of peptide was added to the FlAsH-labeled CaM in the presence of 1 mM $CaCl_2$ and incubated at room temperature for 30 min before photolysis. Authentic C4-CaM in which all methionines were quantitatively oxidized was prepared from FlAsH-labeled C4-CaM by incubation with 50 mM H_2O_2, essentially as described previously (*29*). Deuterium exchange involved reducing the FlAsH-labeled C4-CaM solution to dryness followed by addition of an equal volume of D_2O.

Photolysis. Photolysis experiments were conducted in a Rayonet RPR-200 photoreactor (Southern New England Ultra Violet Co., Branford, CT) equipped with 16 UV lamps centered at 419 nm, where ~90% of the emission is in the 410−450-nm region. At the center of the reactor, the intensity of the emitted light is ~3.1 mW/cm^2 total and 0.15 mW/cm^2 in the 450−480-nm region associated with FlAsH excitation. Quartz test tubes (path length = 0.8 cm) containing FlAsH-labeled or unlabeled CaM (0.1−1 mL) were placed in a merry-go-round device about 2 cm from UV lamps and irradiated for the desired period of time before removing the aliquots for analysis. To exclude oxygen from certain samples, test tubes were capped with rubber septa and evacuated and purged with argon three times at 5 min each before photolysis. For sodium azide inhibition experiments, the desired amount of sodium azide was added to the solution before photolysis. Analyses of products were carried out by SDS−PAGE, HPLC, and mass spectrometry.

Proteolysis. After photolysis, samples were dialyzed into 20 mM ammonium bicarbonate (pH 8.4), from which a 40-μL aliquot was taken, mixed with 1 μg of trypsin (Promega), and incubated at 37 °C for 6−10 h. Peptide mixtures were then subjected to LC−MS analysis without further action.

Fluorescence Correlation Spectroscopy. Correlation spectra [$G(\tau)$] were obtained using a Nikon TE300 inverted microscope modified for these measurements, where excitation was from a Coherent Innova 400 laser (488 nm) focused by a 100× objective lens (S Fluo100, Nikon, Japan). The fluorescence was collected using the same objective, separated by a 505DCLP dichroic mirror (Chroma Technology, Brattleboro, VT), split by a cube beam splitter (Thorlabs, Newton, NJ), and then collected after HQ535 emission filtering (Chroma Technology). The resulting fluorescence was detected by a pair of SPCM-AQR-14 avalanche photodiodes (Perkin-Elmer Optoelectronics, Vaudreuil, Canada). The output was analyzed by a Flex01-05D multi-tau correlator (Correlator.com, Bridgewater, NJ). The collecting time for each curve is 300 s. The autocorrection curves were fit with the "Triplet-State" model by Origin's nonlinear fitting function (MicroCal software, Northampton, MA), where

$$G(\tau) = 1 + \left(1 + \frac{T}{1-T}e^{-\tau/\tau_T}\right)\frac{1}{N}\frac{1}{\left(1+\frac{\tau}{\tau_D}\right)\cdot\sqrt{1+S^2\frac{\tau}{\tau_D}}}$$

N was the total number of fluorescent molecules within the focus point, τ is the log time, and T and τ_T are the fractional population and decay time of the triplet state, respectively. S is the structural parameter of the experimental setup. τ_D is the translational diffusion time of the molecule. The relation between the diffusion time constant and translational diffusion coefficient (D) is

$$\tau_D = \frac{\omega^2}{4D} \tag{2}$$

where ω is the lateral radius of the focus volume (0.46 fL). The measured and theoretical diffusion coefficients can be compared using the Stokes−Einstein formula to estimate the diffusion coefficient of a spherical particle

$$D = \frac{kT}{6\pi\eta R} \tag{3}$$

where k is the Boltzmann constant (1.38×10^{-23} J/K), T is the absolute temperature (293 K), η is the viscosity of water (0.01 P), and R is the hydrodynamic radius of the molecule that can be calculated from the molecular mass (m) using the following formula:

$$R = \sqrt[3]{\frac{3m/N_A}{4\pi\rho}} \tag{4}$$

where N_A is Avogadro's number and ρ is the mean density of the molecule. The masses of fluorescein and FlAsH-labeled CaM are 332 Da and 17 133 Da, respectively.

Electrophoresis. Denaturing and reducing SDS−PAGE was performed using an XCell SureLock Mini-Cell system from Invitrogen (Carlsbad, CA). An aliquot of 5 μL from the 60 μM protein reaction mixture was mixed with 4× NuPAGE LDS sample buffer containing 5% BME (v/v) and heated at 70 °C for 10 min before it was loaded onto NuPAGE precast 12% Bis-Tris gels (Invitrogen) using MES running buffer. The gels were stained using GelCode Blue (Pierce).

Liquid Chromatography. Whole protein analyses of CaM before and after irradiation were carried out on a Zorbax SB-C18 column (4.6 × 150 mm, 3.5 μm particle size) using an Agilent 1100 series LC (Agilent Technologies, Palo Alto, CA) coupled with a diode array UV detector. Proteins (15 μL) were eluted at 30 °C at a flow rate of 1 mL/min with a gradient of 20−60% B in 30 min (A, 0.1% TFA in H_2O; B, acetonitrile) and detected at 210 and 280 nm. Oxidation-induced modifications to CaM were identified by comparison to the elution times of authentic samples of reduced and oxidized C4-CaM, which had retention times of 18.5 and 13.8 min, respectively.

LC−MS and Data Analysis. Trypsinized proteins were analyzed by the Agilent 1100 series LC system in line with a diode array detector monitored at 210 nm and a quadrupole

MS detector with an electrospray ionization source (Agilent LC\MSD SL). Protein digests (20 μL) were separated on the same Zorbax SB-C18 column as described above at 30 °C and a flow rate of 1 mL/min with a gradient change of 5−60% B in 67 min (A, 0.1% TFA in H_2O; B, 90% acetonitrile and 0.1% TFA in H_2O). Data acquisition and analysis were both carried out using Agilent ChemStation software. Peptides were identified by their unique elution times and *m*/*z* values. Quantification of individual peptides was based on the integrated peak area of the selective ion intensity of their mono-charged or double-charged ions. Calculations of *m*/*z* of digested CaM peptides and their modifications were assisted by GPMAW software (Lighthouse Data, Odense, Denmark). The extent of oxidation for each tryptic peptide is calculated as the ratio of the integrated intensities for oxidized peptides to the total amount of the peptide in both oxidized (T_{ox}) and reduced (T_{red}) form as $T_{ox}/(T_{ox} + T_{red})$. For peptides containing multiple methionines, care was taken to correct for the number of oxidized methionines in the peptide and extent of oxidation, calculated as $((T_{ox}/2) + T_{ox2})/(T_{ox} + T_{ox2} + T_{red})$ in the case of two methionines or $((T_{ox}/3) + (2T_{ox2}/3) + T_{ox3})/(T_{ox} + T_{ox2} + T_{ox3} + T_{red})$ in the case of three methionines.

MALDI Mass Spectrometry. A Bruker autoflex MALDI-TOF/TOF mass spectrometer (Bruker Daltonics, Billerica, MA) was used to identify the whole protein mass of CaM before and after FALI. The instrument was calibrated using protein standards (MS-CAL1, Sigma). Using sinapinic acid as matrix (10 mg/mL in 50% acetonitrile and 0.1% TFA), we mixed 1 μL of CaM (60 μM) with 4 μL of matrix, and 1 μL of the mixture was deposited onto a MALDI target plate for analysis. Data analysis was done by FlexAnalysis from Bruker. Mass accuracy was estimated to be ±100 Da in the range of CaM's mass.

Calculations. Surface accessibility and distance to dye of each methionine were calculated from the crystal structure for Ca-bound (1cll.pdb) (*19*) and apo (1cfd.pdb) CaM (*21*). Distances were measured from sulfur atoms on individual methionines to the closest cysteine among the tetracysteine tag using Swiss PdbViewer. Surface accessibility was calculated using the program Surface Racer 3.0 (*30*), with a probe radius corresponding to oxygen of 1.7 Å (*31*). For those peptides containing multiple methionines, the surface accessibilities and intermolecular distances represent the sum of all methioinines and the average distance to the nearest sulfur on the tetracysteine tag.

Affinity Isolation of CaM-Binding Protein. Frozen mouse brains were thawed on ice and placed into a precooled tissue grinder. Samples and buffers were kept on ice throughout the preparation procedure. Tissue was homogenized following addition of lysis buffer [3 mL/brain of 50 mM Tris-HCl (pH 7.4), 150 mM NaCl, 0.1% Triton X-100, EDTA-free Roche complete protease inhibitor cocktail, and 1 mM $CaCl_2$ or 1 mM EGTA]. The homogenate was transferred into Eppendorf tubes and centrifuged at 20 800*g* for 30 min in a tabletop centrifuge at 4 °C to remove cytoskeletal elements. Supernatants were carefully removed without disturbing the pellet and the top lipid layer and were transferred to clean tubes. Brain lysates were incubated for 2 h at 4 °C with Sepharose 4B beads alone or with either wild-type CaM or oxidized CaM (CaM_{ox}) following the oxidation of all nine

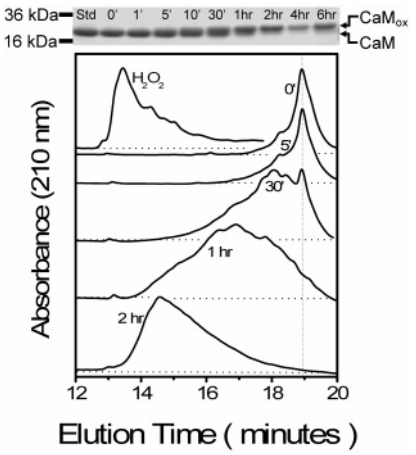

FIGURE 2: Light-induced modification of FlAsH-labeled CaM resolved using (top) SDS−PAGE and (bottom) HPLC for wild-type CaM standard (Std) after 6 h irradiation in comparison to FlAsH-labeled CaM following irradiation (120 fW/fL) for indicated times. For comparison, all methionines in FlAsH-labeled CaM were fully oxidized using H_2O_2. Experimental conditions involved 60 μM CaM in 20 mM HEPES (pH 7.6), 150 mM NaCl, 1.0 mM $CaCl_2$, and 5 mM BME.

methionines by hydrogen peroxide (*29*). Following gentle rotation in the presence of 1 mM $CaCl_2$ or 1 mM EGTA, beads were washed five times with lysis buffer [50 mM Tris-HCl (pH 7.4), 150 mM NaCl, and 0.1% Triton X-100] containing 1 mM $CaCl_2$ or 1 mM EGTA, and bound proteins were resolved by SDS−PAGE. To elute samples, 50−100 μL of elution buffer (4.0 M urea, 10 mM EGTA, and 5 mM DTT) was added to the beads, and the samples were incubated at 90 °C for 5 min with occasional vortexing. The eluted material was separated from the beads by centrifugation at 20 800*g* for 1 min and resolved by SDS−PAGE.

RESULTS

Light Sensitivity of FlAsH-Labeled CaM. Following labeling of helix A of C4-CaM with FlAsH (Figure 1), we observed that upon illumination of the sample (120 μW/mL) there is a progressive decrease in the mobility of FlAsH−CaM on SDS−PAGE (Figure 2). Despite the low power of the irradiated light, there is a significant band broadening that is apparent following 10 min of illumination. More extended irradiation was necessary for a complete shift to the upper band. In contrast, there is no change in the mobility of the unlabeled C4-CaM standard following illumination for 6 h, indicating that the FlAsH fluorophore is responsible for the observed structural change. This diminished mobility on SDS−PAGE is analogous to what is observed following the in vitro oxidation of wild-type CaM using hydrogen peroxide or under conditions of oxidative stress in vivo (*32*, *33*). Similar light-induced shifts in the elution time of FlAsH-labeled CaM are apparent using reversed-phase liquid chromatography, where irradiation results in a reduction in the elution time that approaches that associated with a fully oxidized CaM standard prepared following exposure to hydrogen peroxide. These results suggest that CaM is sensitive to FALI, which is likely to involve the oxidative modification of the protein.

Identification of Reactive Oxygen Species. We probed the mechanism underlying light-induced changes in CaM structure by substituting oxygen in solution with argon, which

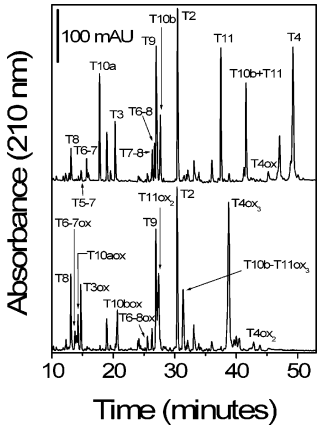

FIGURE 3: HPLC tryptic digest of FlAsH-labeled CaM before (top) and after (bottom) 2 h of irradiation, with peak identifications of individual tryptic fragments obtained from mass spectrometric analysis, as detailed in Table 1. In the bottom chromatograph, peak T5−7ox was identified between T6−7ox and T10aox, but was not labeled due to peak crowding in that region. Tryptic fragment corresponding to FlAsH-labeled T1 fragment has a delayed retention time and is not shown.

abolishes light-induced mobility shifts and changes in the elution times of FlAsH-labeled CaM (data not shown). Additional resolution of the role of oxygen involved light exposure of FlAsH-labeled CaM in deuterated water buffer, where an approximately 2-fold rate enhancement is observed. These results implicate singlet oxygen as the reactive species, because deuterated solvents selectively extend the lifetime of singlet oxygen and have no effect on hydroxyl radicals (*12*, *34*). Consistent with an important role for singlet oxygen, we find a 70% and 90% reduction, respectively, in the rate of CaM modification in the presence of sodium azide (Supporting Information, Figure 2), which is a singlet oxygen quencher (*5*).

Identification of Modification Sites. To assess the modification sites in CaM following illumination, CaM was proteolytically digested and the resulting peptides were subjected to LC separation and in-line mass spectrometric identification. Prior to illumination, 14 major peaks were identified with authentic tryptic cleavage sites that elute within the first hour (Figure 3; Table 1). An additional major peak associated with the FlAsH-labeled peptide (i.e., Ala^{1} to Lys^{13}) eluted at considerably longer times (data not shown). These resolved peaks account for the entire CaM sequence; unidentified peaks correspond to peptides with nontryptic cleavages or other impurities. Following light exposure, there are significant changes in the elution times of all methionine-containing peptides in the chromatogram (i.e., T3, T4, T5−7, T6−7, T10a, T10b, and T11). Mass spectrometric analysis of the peaks in the tryptic digest following light exposure indicates that the integrated areas of the parent peptides that are diminished following light exposure contain additional masses in multiples of 16 amu, which correspond to methionine sulfoxides (Table 1). Excluding the unidentified peaks that also appear in the control sample, remaining unidentified new peaks that are apparent following light exposure account for $<5\%$ of the total peak area, as measured by absorbance at 210 nm. Masses of these unidentified peaks were compared with hypothetical masses of other possible oxidation products; however, no further oxidation products were identified. Thus, methionine oxidation is the main oxidative modification generated following light exposure of CaM.

Additional reactive amino acids may not generate stable photoproducts upon illumination of FlAsH-labeled CaM, which results in a range of poorly defined peptide masses. Therefore, we have investigated possible decreases in the integrated peak intensities associated with the majority of resolved peptides (Figure 4). In this analysis, we paid special attention to peptides containing amino acids known to be oxidatively modified, which include methionine, histidine, and tyrosine (*35*). In the case of the two tyrosines, Tyr99 is located in the T9 peptide that contains no methionines and whose integrated intensity is unchanged following illumination of FlAsH-labeled CaM. The other tyrosine (Tyr138) is within peptide T11 together with two methionines. The oxidized peptide $T11ox_2$ is repeatedly detected as a double peak with the same mass, probably because the two neighboring oxidized methionines (sulfoxides) in peptide T11 exist in two different stereo structures that have distinct conformations in solution (*36*, *37*). If this is taken into account, we find that the peaks corresponding to both Tyr138-containing tryptic peptides, that is, T10b + T11 and T11, also shift to their methionine-oxidized products with comparable peak area before and after illumination. This stability of the total peak area of tyrosine-containing peptides and the fact that no new peaks with tyrosine oxidation products can be identified indicate that tyrosines are stable under these reaction conditions.

In contrast to all other peptides identified in the chromatogram, there is a $66 \pm 4\%$ decrease in the integrated intensity associated with T10a and, to some extent, modest decreases in the integrated areas of proximal peptides to T10a within the primary sequence of CaM. Identification of the modified amino acid within T10a is facilitated by prior knowledge of oxidatively sensitive amino acids in CaM. T10a contains both methionine and histidine side chains. T10aox shows the expected shift on the chromatogram due to methionine oxidation found for all methionine-containing peptides. However, the decrease of the peak intensity before and after oxidation to less than 35% of the original is unique to this peptide (Figure 4). Because T10a is the only histidine-containing peptide in CaM and contains no other amino acids that are not duplicated elsewhere in the CaM sequence, this is a good indication that the loss of peptide is due to histidine modification. As discussed above and shown in Table 1 and Figures 3 and 4, we were able to account for methionine oxidations by identifying peptides with an added mass of 16 and subsequently used peak intensities to verify that the tyrosines in the sequence were not modified. In contrast to methionine oxidation, our inability to identify any products associated with histidine oxidation in the tryptic map of C4−CaM following illumination is unsurprising, as associated oxidation products are known to be complex and the yield of each oxidation product would be expected to be small (*38*).

Oxidation Kinetics. The kinetics of methionine oxidation associated with light exposure was measured for all resolved peaks in the tryptic digest for both apo- and calcium-activated CaM. Following light exposure for the indicated times, samples were collected and subjected to tryptic digestion and LC−MS analysis. On the basis of the ion intensity of the oxidized peptide versus unoxidized peptide in the mass

Table 1: Mass Spectrometric Identification of Tryptic Peptides Isolated from CaM[a]

tryptic fragment[b]	sequence	$[M + 2H]^{2+}$ observed	$[M + 3H]^{3+}$ observed	$[M + H]^{+}$ theoretical	$[M + H]^{+}$ experimental	error (Da)
T2	$Glu^{14}-Lys^{30}$		615.6	1844.89	1844.78	0.11
T3	$Glu^{31}-Arg^{37}$	403.2		805.42	805.39	0.03
T3 (SO)	$Glu^{31}-Met(O)-Arg^{37}$	411.2		821.42	821.39	0.03
T4	$Ser^{38}-Arg^{74}$		1357.35	4069.85	4070.03	−0.18
T4 $(SO)_1$	$Ser^{38}-Met(O)-Arg^{74}$		1362.7	4085.84	4086.08	−0.24
T4 $(SO)_2$	$Ser^{38}-Met(O)_2-Arg^{74}$		1367.9	4101.84	4101.68	0.16
T4 $(SO)_3$	$Ser^{38}-Met(O)_3-Arg^{74}$		1373.4	4117.83	4118.18	−0.35
T5−7	$Lys^{75}-Arg^{86}$		494.2	1480.70	1480.58	0.12
T5−7(SO)	$Lys^{75}-Met(O)-Arg^{86}$		499.6	1496.69	1496.78	−0.09
T6−7	$Met^{76}-Arg^{86}$	676.8		1352.60	1352.59	0.01
T6−7 (SO)	$Met^{76}-Met(O)-Arg^{86}$	684.7		1368.60	1368.39	0.21
T6−8	$Met^{76}-Arg^{90}$	928.2		1855.85	1855.39	0.46
T6−8 (SO)	$Met^{76}-Met(O)-Arg^{90}$	936.2		1871.84	1871.39	0.45
T7−8	$Asp^{78}-Arg^{90}$		532.8	1596.71	1596.38	0.33
T8	$Glu^{87}-Arg^{90}$			522.27	522.2	0.07
T9	$Val^{91}-Arg^{107}$		585.65	1754.87	1754.93	−0.06
T10a	$His^{107}-Lys^{115}$	514.6		1028.52	1028.19	0.33
T10a (SO)	$His^{107}-Met(O)-Lys^{115}$	22.6		1044.51	1044.19	0.32
T10b	$Leu^{116}-Arg^{126}$	675.2		1349.63	1349.39	0.24
T10b (SO)	$Leu^{116}-Met(O)-Arg^{126}$	683.2		1365.62	1365.39	0.23
T10b-11	$Leu^{116}-Lys^{148}$		1274.3	3820.69	3820.88	−0.19
T10b-11 $(SO)_3$	$Leu^{116-}Met(O)_3-Lys^{148}$		1290.6	3868.67	3869.78	−0.11
T11	$Glu^{127}-Lys^{148}$	1245.6		2490.08	2490.19	−0.11
T11 (SO)	$Glu^{127}-Met(O)-Lys^{148}$	1253. 5		2506.08	2505.99	0.09
T11 $(SO)_2$	$Glu^{127}-Met(O)_2-Lys^{148}$	1261.7		2522.07	2522.39	−0.32

[a] All peptide ions in this ESI-MS experiment were detected with an accuracy within 0.032% of the theoretical mass of the peptide of interest; there were no ambiguities in peptide assignment. [b] Elution time of FlAsH-labeled T1 peptide was reduced substantially and not routinely detected.

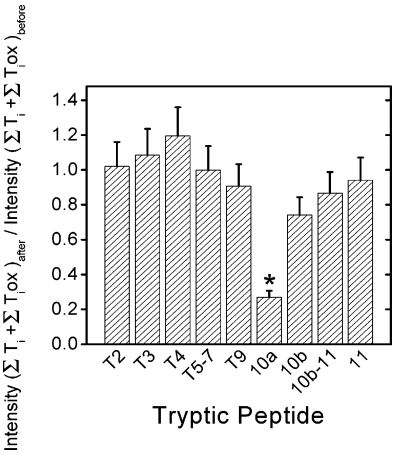

FIGURE 4: Quantitation of recovered peptides following 2 h of light exposure, taking into account the full range of recovered peptides following oxidative modification. Quantitation involved integration of absorption peaks for each tryptic peptide (see Figure 3).

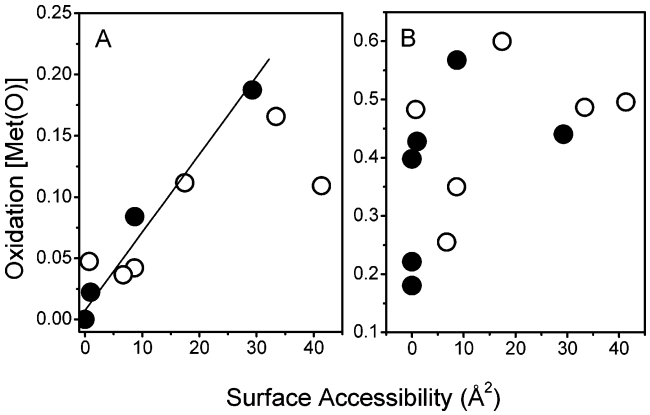

FIGURE 5: Correlation between extent of methionine oxidation and calculated surface accessibility following (A) 5 and (B) 60 min of light exposure for apo-CaM (closed circle) and calcium-activated CaM (open circle). Experimental conditions involved 60 μM CaM in 20 mM HEPES (pH 7.6), 150 mM NaCl, 5 mM BME, and either 1.0 mM EGTA (apo-CaM) or 1.0 mM $CaCl_2$ (calcium-activated CaM). Surface accessibilities were calculated from either 1cll.pdb (*30*) or 1cdf.pdb (*21*) using the program Surface Racer 3.0 (*32*).

chromatogram, the percentage of methionines oxidized for each tryptic peptide was determined. In the cases of peptides containing multiple methionines (i.e., T4 and T11), the extent of oxidation was corrected for the total number of methionines. Initial rates of oxidation, measured at 5 min following light exposure, demonstrate a linear relationship between oxidation rates and the calculated surface accessibility for singlet oxygen (radius = 1.7 Å) from the high-resolution structures for the majority of resolved peptides in both the apo- and calcium-activated forms of CaM (Figure 5). We note that the calculated surface accessibility of one point—corresponding to T11 in the calcium-activated form of CaM—that falls off the line is incorrect; molecular dynamic measurements indicate that the surface accessibility of these methionines is 21 $Å^2$ (*39*). There is no correlation between initial rates of oxidation and the intermolecular distance between FlAsH and the sulfur moieties on individual methionines (Table 3). Given the large differences in the surface accessibilities for individual methionines in the apo- and calcium-bound forms of CaM, these results indicate that following light exposure, singlet oxygen diffusion is fast compared to the rate of chemical modification. At longer times (i.e., 2 h) of illumination, the extent of methionine oxidation in all tryptic fragments is increased. The linear correlation between the extent of oxidation and surface accessibility apparent from the initial rates is diminished, consistent with prior measurements indicating that methionine oxidation disrupts the tertiary structure of CaM to result in a conformationally unstable molten globule state (*33*, *40*, *41*).

Table 2: Excited-State Lifetime and Diffusion Constants from Fluorescence Correlation Spectroscopy[a]

	fluorescein		CaM-FlAsH	
oxyrase (O_2 consuming enzyme mixture)	−	+	−	+
fluorescence intensity (cps) $\times 10^{-3}$	66 ± 2	88 ± 1	3.5 ± 0.4	12.9 ± 0.5
brightness (cps/molecule) $\times 10^{-3}$	4.72 ± 0.06	4.55 ± 0.01	1.30 ± 0.03	1.21 ± 0.03
triplet lifetime (μs)	1.9 ± 0.1	2.4 ± 0.2	3.3 ± 0.8	3.4 ± 0.6
triplet fraction	0.31 ± 0.01	0.28 ± 0.02	0.35 ± 0.03	0.42 ± 0.05
diffusion time, τ_D (μs)	47.3 ± 0.4	50.0 ± 0.6	160 ± 6	174 ± 4
calculated translational diffusion coefficient, D_t ($cm^2\ s^{-1}$) $\times 10^6$	4.08 ± 0.04	4.06 ± 0.03	1.15 ± 0.03	1.17 ± 0.04

[a] Errors are standard errors of the mean; $n > 8$; measurements involved data collection for 5 min using 0.1 mL of either 1 nM fluorescein or 20 nM FlAsH-labeled CaM in 10 mM K_2HPO_4 (pH 7.2), 0.15 M NaCl, 0.2 mM NaN_3, and when indicated 0.03 units of oxyrase in the presence of 10 mM lactate.

Table 3: Calculated Physical Properties and Extent of Oxidation for Individual Methionines within Each Tryptic Peptide from CaM

	Ca-bound CaM[a]				Apo-CaM[a]			
			conversion (%)				conversion (%)	
trypsin peptide ID	SA[b] (Å^2)	distance[c] (Å)	5 min	60 min	SA[b] (Å^2)	distance[c] (Å)	5 min	60 min
T3	6.697	19.0	3.6	25.5	10.3	0	0	18.0
T4	17.445	14.2	11.1	60.0	12.6	2.898	8.4	56.7
T6	33.40	8.0	16.6	48.6	7.4	29.28	18.7	44.0
T10a	0.735	37.7	4.7	48.2	20.3	0	0	22.1
T10b	8.657	40.4	4.2	35.0	18.1	0	0	39.8
T11	41.38	34	10.9	49.5	18.9	0.489	2.2	42.8

[a] All properties are calculated from the structure 1CLL for Ca-bound CaM and 1CFD for apo-CaM. [b] Accessibility is calculated by program Surface Racer 3.0 (*30*) using oxygen as probe size, 1.7 Å (*31*). Surface accessibilities of those peptides containing multiple methionines are the sum of the surface accessibility of all methionines. [c] Distances are measured from the S atom on methionine to the closest cysteine among the tetracysteine tag using Swiss PdbViewer (*64*). Distances are calculated as an average of all methionines in multiple-methionine peptides.

Excited-State Lifetimes. Additional resolution regarding the mechanism of reactive oxygen species generation associated with the oxidation of CaM was investigated using fluorescence correlation spectroscopy (*42*) to directly measure the excited triplet state of FlAsH-labeled CaM, and through a comparison with that of free fluorescein, whose mechanism underlying FALI has been extensively studied and is known to involve singlet oxygen (*7*, *10*). A consideration of the autocorrelation function [$G(\tau)$] for fluorescein with that of FlAsH-labeled CaM demonstrates that there is a significant shift toward longer times relative to the free chromophore. In both cases, the autocorrelation functions can be adequately fit using two constants corresponding to the triplet lifetime and the translational diffusion coefficient, as demonstrated by the randomly weighted residuals (Figure 6). In comparison to the 50 μs time constant for fluorescein, the diffusional time is increased by approximately 3.4-fold for FlAsH-labeled CaM to approximately 170 μs (Table 2). The calculated translational diffusion coefficients (D) from these time constants (τ_D) are 4.1×10^{-6} and 1.2×10^{-6} $cm^2\ s^{-1}$ for fluorescein and FlAsH-labeled CaM, respectively. These values are in good agreement with the theoretical values, which are respectively 4.5×10^{-6} and 1.2×10^{-6} $cm^2\ s^{-1}$. Thus, the measured diffusion coefficients are consistent with the molecular sizes of fluorescein and FlAsH-labeled CaM and provide increased confidence that the fits to the data accurately measure the excited-state properties of these chromophores.

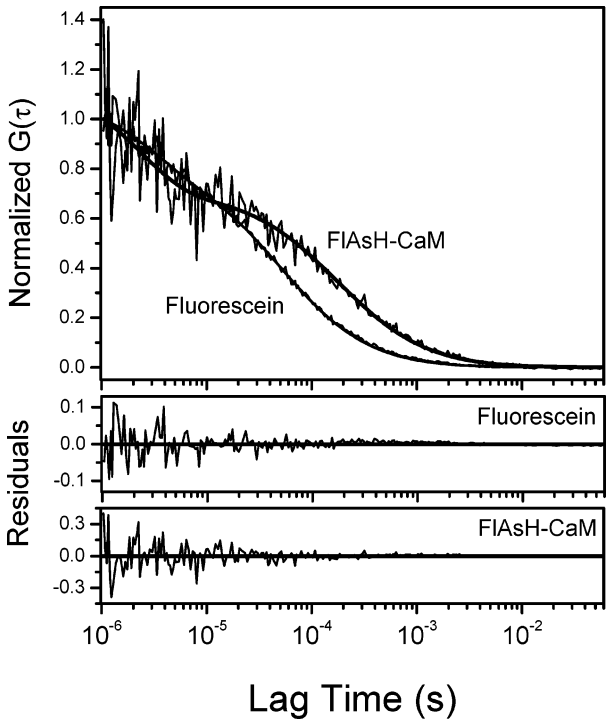

FIGURE 6: Normalized autocorrelation data and nonlinear least-squares fits, comparing fluorescein and FlAsH-labeled CaM (top) and associated residuals (bottom). Experimental conditions involved 1 nM fluorescein or 20 nM FlAsH-labeled CaM in 10 mM K_2HPO_4 (pH 7.2), 0.15 M NaCl, and 0.2 mM NaN_3 at 20 °C. Laser was focused 50 μm above a freshly cleaned cover slip, prepared by sonicating cover slips in 10% NaOH for 20 min followed by 15 min of sonication in acetone. Acquisition time was 5 min.

From the least-squares fits to the data, it is apparent that the amplitudes and lifetimes of the triplet states of fluorescein and FlAsH-labeled CaM are very similar, although fluorescein is much brighter than FlAsH-labeled CaM because of the fluorescence quenching by the arsenic moieties. Enzymatic reduction of the oxygen concentration upon addition of Oxyrase prevents photobleaching associated with the generation of singlet oxygen, resulting in an increase in fluorescence intensity from the larger number of molecules in the focal volume with little change in the brightness of individual fluorophores (Table 2). Decreasing the concentration of molecular oxygen also results in significant increases in the triplet state that is most pronounced for the free dye, consistent with prior suggestions that singlet oxygen is generated upon the collisional interaction between oxygen and fluorophores in the first excited triplet state (*10*, *43*, *44*).

Photo-Cross-Linking in the Presence of Binding Partners. Additional resolution regarding the sensitivity of CaM to

light-induced oxidative modification was assessed following association with the CaM-binding sequences of different target proteins: myosin light chain kinase from rabbit (MLCK) (*24*) and human (MLCK*) smooth muscle (EC2.7.1.117), the plasma membrane Ca-ATPase (C28W) (*25*), and the RyR calcium release channel (*26*). Irrespective of the CaM-binding peptide, there is a reduced mobility of the band corresponding to CaM on SDS−PAGE whose apparent molecular mass changes from 16 to 20 kDa after 2 h of light exposure, indicating that CaM remains sensitive to oxidative modification irrespective of target peptide binding (data not shown). Nevertheless, compared to the FALI of CaM alone, a much slower oxidation rate was observed for peptide-bound CaM within the initial 30 min of light illumination (data not shown), which is consistent with previous studies where methionines in CaM are not oxidized when complexed to a peptide following exposure to peroxynitrite (*45*, *46*). In addition, in the cases of MLCK and RyR, an additional band is apparent above that of CaM with respective apparent masses of ~23 and 26 kDa. As shown in Figure 7, these bands are even more pronounced after 6 h of irradiation, and higher mass species are beginning to appear for the MLCK* and C28W binding peptides. The additional mass of the new bands is consistent with that of the CaM adduct, suggesting that cross-linking was induced under the described FALI conditions and may contribute to the mechanism of protein inactivation. Formation of the cross-linked product was confirmed for the complex between CaM and MLCK using MALDI mass spectrometry, where it is apparent that the mass of the cross-linked complex (i.e., 19 500 ± 100 Da) corresponds to that of FlAsH-labeled CaM and MLCK whose theoretical average mass is 19 428. While we were unable to identify the site of cross-linking, it is significant that MLCK and RyR, which contain histidines in the binding site, produce significantly more cross-linked peptide in a shorter time than MLCK* and C28W. Given that, especially between MLCK and MLCK*, there are no other significant differences in amino acid composition and that the histidine side chain in CaM is itself sensitive to light-induced chemical modification, these results suggest that the histidine within the binding site may participate in photoactivated cross-linking, as previously suggested for other proteins (*9*, *38*). The cross-linked species for the control peptides indicate that, while the majority of the cross-linking may stem from the active site histidine, either the histidine in calmodulin or other amino acids also contribute to the formation of cross-linked species.

Finding intermolecular cross-links caused us to look for intramolecular cross-links in the FALI reaction without binding partners, which might have escaped notice. Because of the good recovery of all peptides but T10a after photolysis, we speculated that the histidine in T10a is the most possible initiator of intramolecular cross-linking. We then examined CaM's crystal structures for the residues most reactive toward photooxidized histidine intermediate near His107, that is, lysines, cysteines, tyrosines, and arginines, and found them to be located in T9, T10a, and T10b. On the basis of the earlier mechanistic studies of histidine-induced cross-linking (*47*, *48*), we calculated the theoretical masses of predicted intramolecular cross-linking and searched for those masses in the LC−MS data; however, no evidence of intramolecular cross-linking was found. Examination of the crystal structure,

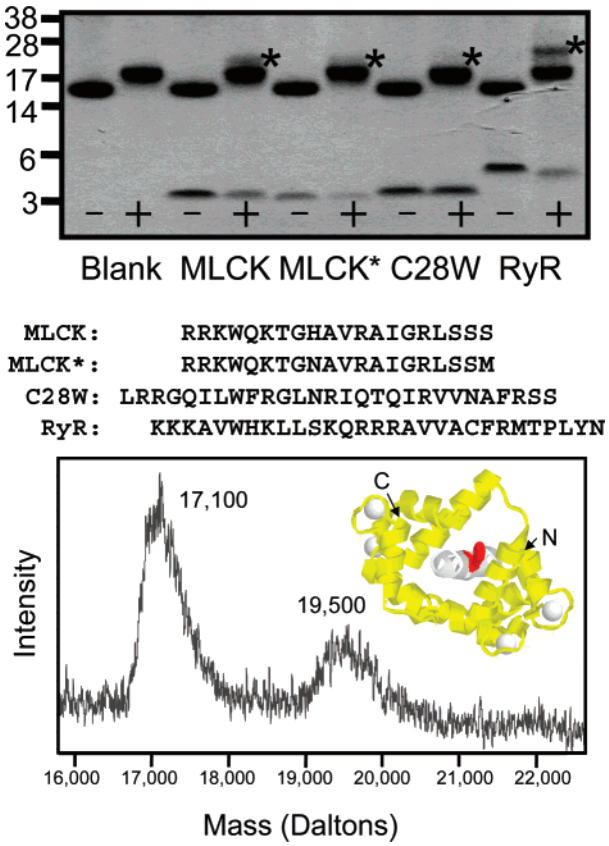

FIGURE 7: Selective cross-linking between FlAsH-labeled CaM and CaM-binding peptides. (Top) SDS−PAGE of FlAsH-labeled CaM incubated in the presence of peptides corresponding to the CaM-binding sequence of the myosin light chain kinases from rabbit (MLCK) and human (MLCK*), the plasma membrane Ca-ATPase (C28W), and the RyR calcium release channel following 6 h of incubation in either the dark (−) or following light exposure (+). (Bottom) MALDI mass spectrum of intact FlAsH-labeled CaM following incubation with CaM-binding sequence from MLCK, where the theoretical average masses of the MLCK peptide, C4-CaM, FlAsH-labeled CaM, and the FlAsH-labeled CaM + MLCK peptide complex are 2295, 16 657, 17 133, and 19 428 Da, respectively. Species detected include the unbound MLCK (not shown in the spectrum), FlAsH-labeled C4-CaM (17 100 Da), and its cross-linked complex with MLCK peptide (19 500 Da). Experimental masses are within the instrument error of ±100 Da and consistent with theoretical calculations. (Inset) Ca-CaM (yellow) binding the MLCK peptide (white with red His side chain) (1 cdl.pdb).

which places His107 in solution rather than near a nucleophilic amino acid on the chain, also substantiates the above supposition that hydrolysis is the most likely fate of the oxidized histidine species in this case.

Fluorophore-Activated Light Inactivation of CaM Function. The oxidation of methionines in CaM has previously been shown to result in the functional inactivation of the plasma membrane Ca-ATPase and to selectively diminish binding affinity in other target proteins (*32*, *40*, *49*−*51*). To investigate the generality of this prediction, we have compared the calcium-dependent binding of wild-type and oxidized CaM (in which all nine methionines were quantitatively oxidized to their corresponding sulfoxides) to target proteins present in brain lysate. Under these conditions, we observed a significant number of binding targets that associate with immobilized wild-type CaM in a calcium-dependent manner (Figure 8C). Following oxidation, we observed a dramatic reduction in the number and intensity

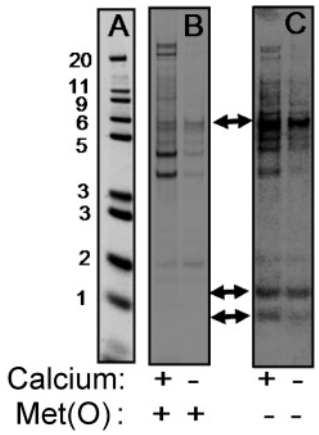

FIGURE 8: Visualization of binding partners to oxidized (B) and wild-type (C) apo- and calcium-activated CaM following affinity pull-down and elution from CaM−sepharose beads incubated with lysate from mouse brain in 50 mM Tris-HCl (pH 7.4), 150 mM NaCl, and 0.1% Triton X-100 in the presence of either 1.0 mM $CaCl_2$ or 1.0 mM EGTA. Panel A shows molecular mass markers and their corresponding masses in kilodaltons.

of binding partners (Figure 8B). Because under normal conditions CaM concentrations are limiting relative to binding partners (*52*−*55*), these results indicate that the light-induced oxidation of CaM will result in an inability to bind and activate the majority of target proteins.

DISCUSSION

Fluorophore-assisted light inactivation (FALI) is an attractive method for disabling the functional activity of CaM and other essential proteins in vivo after protein synthesis and localization, and it provides a means of protein inactivation that has important advantages over other traditional approaches involving gene ablation or silencing methods. FlAsH-labeled CaM is readily oxidized (Figure 2), resulting in an inability to bind and activate the vast majority of CaM-binding proteins (Figure 8). Modifications associated with photoinactivation primarily stem from a singlet oxygen mechanism that results in the oxidation of methionine to its corresponding methionine sulfoxides and can induce cross-linking to proximal amino acids, which appear to stem mainly from histidine oxidation products (Figures 3 and 7; Table 1). The extent of methionine oxidation is dependent on the surface accessibility of individual methionine sulfurs (Figure 5A); there is no relationship between the extent of methionine oxidation and the intermolecular distance between methionines and the FlAsH chromophore (Figure 5; Table 3). These latter results indicate that the rate of singlet oxygen diffusion is fast compared to the rate of reaction and suggest principles that can be applied in both the choice and design of proteins for light-induced photoinactivation.

Identification of Photoinduced Reactive Species and Functional Implications for Protein Inactivation. Photoinduced reactive species associated with protein inactivation are likely to involve either hydroxyl radicals or singlet oxygen, which have, respectively, been previously implicated in the photoinactivation of several proteins using either malachite green or various fluorescent chromophores (*5*, *11*, *12*). In the case of FlAsH-labeled CaM, we have shown that photoinactivation occurs primarily through a singlet oxygen mechanism whose rate of formation is sensitive to changes in oxygen concentration, the presence of D_2O, and azide quenching. This mechanism is similar to that associated with fluorescein (*10*), indicating that while the arsenic ligands on FlAsH modulate its fluorescence intensity and brightness the same basic excited-state mechanism applies involving the formation of a long-lived triplet state common to fluorescein (Table 2). This means that the mechanistic findings contained herein can be extended to FALI using FITC-labeled antibodies or proteins.

In comparing the properties of singlet oxygen and hydroxyl radicals, the implications of a singlet oxygen-catalyzed mechanism in modulating protein function under in vivo conditions can readily be recognized, because hydroxyl radicals are far more reactive than singlet oxygen (*53*). Indeed, hydroxyl radicals are inherently nonspecific; that is, all amino acids side chains and backbones as well as nonprotein cellular species are reactive. Thus, a rapid reaction of hydroxyl radicals will occur at the site of generation, resulting in a half-life in the subnanosecond regime. As a result, large amounts of nonspecific damage to sites nearest the sensitizing species will occur that result in a limited photoinactivation of targeted proteins under all but the highest light levels. These limitations are particularly problematic if there is an antibody spacer between the chromophore and the protein of interest, or if the chromophore is not near a functionally sensitive site on the protein. These conclusions are corroborated by data using malachite green, in which the efficiency of protein inactivation declined drastically with increasing distances; no further inactivation was observed beyond a distance between 1.5 and 6 nm irrespective of the light intensity that prevented the inactivation of multiple protein of interest (*11*, *12*).

In contrast, photogeneration of the less-reactive singlet oxygen leads to an enhanced ability for targeted protein inactivation, permitting the selective oxidation of methionines commonly observed at binding interfaces (*56*) and the formation of intermolecular cross-links between the protein under study and its binding partners, as well as possible intramolecular cross-links. Indeed, the lifetime of singlet oxygen in water is approximately 3 μs, corresponding to a calculated diffusion range of approximately 160 nm (*44*). The density of macromolecules inside a cell results in a significantly lower lifetime, estimated to be approximately 250 ns, which limits the diffusion of generated singlet oxygen to about 45 nm (*44*). In agreement with these calculated diffusion ranges, there is no relationship between reactivity and the intermolecular distance between FlAsH and rates of methionine oxidation (Table 3); rather, initial rates of reaction are linearly dependent on surface accessibility (Figure 5A). Thus, the use of engineered tags that permit the direct attachment of multiuse affinity probes on the protein of interest without the need for an intervening antibody in conjunction with the use of photogenerated singlet oxygen will permit the oxidative modification and inactivation of both the protein of interest and its associated binding partners to effectively knock out a pathway of interest. In this latter respect, it is expected that this methodology will permit the identification of conserved hypothetical protein function through the ability to rapidly modulate their function.

Identification of Modification Sites Associated with Singlet Oxygen Generation. Prior measurements have investigated the reactivity of individual amino acids with singlet oxygen

and have identified a sensitivity of histidine, methionine, and tyrosine side chains to oxidative modification, where $k_{His} = 2 \times k_{Met} = 4 \times k_{Tyr,}$ with rate constants on the order of 10^7 $dm^3\ mol^{-1}\ s^{-1}$ (*35*, *57*). Consistent with these expectations, we found that the light-induced generation of singlet oxygen for FlAsH-labeled CaM results in the extensive oxidation of methionine side chains to their corresponding methionine sulfoxides. For the vast majority of peptides, product ions were identified, and we were able to account for 95% of the integrated intensity associated with the parent tryptic peptides prior to illumination (Figure 4). Notably, the products associated with tryptic peptide T10a were largely not accounted for, consistent with the expected reactivity of the single His-107 side chain in CaM that would yield a range of derivatized products that could not be identified by LC−MS. Significantly, there is a corresponding loss in the integrated intensity associated with proximal tryptic peptides (e.g., T10b; Figure 4), suggesting a possible reactivity with the activated histidine. The fact that only 34% of the His-containing tryptic peptide T10a was identified to be methionine-oxidized, while the rest is missing, is consistent with prior measurements that the rate of histidine modification by singlet oxygen is twice that of methionine oxidation (i.e., $k_{His} = 2 \times k_{Met}$) (*35*, *57*). In contrast to initial expectations, we were able to fully account for the two tyrosine-containing peptides T9 and T11, where no significant level of modification for these highly surface-exposed amino acids was identified. These latter results suggest that the mechanism of CaM oxidation is predominantly electrophilic reactions driven by singlet oxygen as opposed to radical-like chemistry induced by superoxide, hydrogen peroxide, or hydroxyl radical, where the oxidation rate of tyrosine is comparable to histidine and faster than methionines (*53*). Differences between the reactivity of tyrosines in intact proteins relative to that reported for isolated amino acids may have been, in part, related to buffer conditions associated with oxidation and low solubility in water (*57*).

FALI Mechanism of CaM. Methionine oxidation is the overwhelming source of modification sustained by CaM in the course of FALI (Figure 3; Table 1). The FlAsH attachment site is located on helix A of CaM (Figure 1) and is not within the interaction sites associated with the ability of CaM to bind target proteins. It has previously been shown that the abilities of both the unlabeled and FlAsH-labeled C4-CaM to fully activate target proteins are comparable to that of the wild-type CaM (*14*). This implies that minimal structural perturbations to CaM are introduced by the tetracysteine tag and FlAsH binding prior to FALI. The almost linear correlation between initial rates of methionine oxidation and the calculated surface accessibility of the sulfur atoms within individual methionines suggests that the structure of CaM is not disturbed by FALI initially when <20% methionine oxidation has taken place (Figure 5A). At longer times, when the extent of oxidation is increased, the correlation between the extent of oxidation and calculated surface accessibility is less pronounced (Figure 5B). These latter results are consistent with prior measurements indicating that methionine oxidation disrupts the structure of CaM to induce a molten globule state with an altered surface accessibility (*33*, *49*). These structural changes are believed to be triggered by an increase in hydrophilicity and proneness for hydrogen bonding of methionine residues after being oxidized to sulfoxides, thus, changing their helix propensities and interhelical packing to increase the surface accessibilities of the methionines in oxidized CaM from the originally calculated values (*49*).

Some useful generalizations are apparent from these measurements regarding the targeted oxidation of critical methionines and functional inactivation of proteins. Prior in vitro measurements using different reactive oxygen species have demonstrated that long-lived reactive species such as hydrogen peroxide selectively oxidize methionines in CaM and, like the current measurements associated with singlet oxygen, there is a linear correlation between the extent of oxidative modification and the surface accessibility (*39*). Indeed, an initial functional screen to access the sensitivity of a given protein to hydrogen peroxide exposure will provide valuable information regarding the likelihood that this protein will be a useful target of FALI. In contrast, highly reactive species such as peroxynitrite have much shorter lifetimes, and these anions can result in a more selective oxidation of specific methionines (i.e., Met^{144} and Met^{145}) in CaM and other proteins. Likewise, hydroxyl radicals are sufficiently reactive that they essentially react at the site of generation (*13*) and have limited selectivity that results in limited use in the design of photoinactivation strategies.

The functional sensitivity of CaM to FALI is apparent both from a consideration of the inability of oxidized CaM to bind to a range of different target proteins (Figure 8) and from prior measurements that have assessed how oxidation may modulate the function of key target proteins, including the plasma membrane Ca-ATPase, the RyR calcium release channel, and nitric oxide synthases (*32*, *51*, *58*−*60*). In the case of the Ca-ATPase, oxidized CaM binds nonproductively and blocks functional activation (*32*, *40*, *50*, *51*), while in the case of the RyR, oxidized CaM prevents channel activation (*58*, *59*). The ability of oxidized CaM to bind in a nonproductive conformation that locks target proteins in an inactive state suggests that some target proteins that retain CaM-binding affinity following FALI are inactive (Figure 8). In contrast, the oxidation of methionines in CaM primarily reduces the binding affinity to nitric oxide synthase, consistent with the vast majority of target proteins that no longer associate with oxidized CaM. These prior measurements, coupled with the demonstration that tagged CaM can be selectively labeled with FlAsH in living cells (*15*), indicate that FALI can be used to investigate cellular networks associated with CaM signaling. We note that, in this respect, relatively low light levels were used in these measurements to permit the kinetic characterization associated with the oxidation of CaM (Figure 5 and Supporting Information). Under these conditions, we exposed FlAsH-labeled CaM to approximately 120 μW of light per milliliter of reaction medium (450−480 nm). Because an average cell has a volume of approximately a femtoliter, these results suggest that 120 fW of light can effectively oxidize CaM in about 10 min. These calculations indicate that FALI is a viable mechanism to modulate protein function, consistent with the reported ability to modulate the function of connexin43 and L-type calcium channels (*5*).

Photoinactivation in the Presence of Binding Partners. Photoactivated cross-linking reactions, either internally or to a binding partner, could be another source of inactivation. In addition, photo-crosslinking reactions have utility to the

researcher by offering the potential to trap protein complexes prior to cell disruption and permit the identification of unstable protein complexes following cell disruption and mass spectrometric identification. Numerous instances of photoinduced protein crosslinking and formation of aggregated products have been reported in the literature; however, the mechanistic pathways are highly dependent on the nature of photosensitizers and proteins used (*35*). Primary examples of photoactivatable cross-linking reactions include the formation of dityrosine cross-links after tyrosine is photosensitized to phenoxyl radicals and cross-linking is induced by oxidized histidines (*47*, *61*). Indeed, following exposure to ultraviolet light, the two tyrosines in CaM are cross-linked in a dityrosine adduct with low efficiency (*62*). Dityrosine cross-linking is usually produced in the so-called direct pathway, in which the excited triplet state of the dye reacts directly with the target molecule by H atom abstraction or electron transfer to produce highly reactive oxidizing species such as superoxide, hydrogen peroxide, and hydroxyl radicals. However, as evidenced from our earlier discussions, FALI of FlAsH-labeled CaM mainly takes place through a singlet oxygen mechanism that results in methionine sulfoxide formation and the generation of reactive histidine intermediates that form a range of products that were not identifiable (Figure 4). Under these conditions, tyrosines are unaffected and form no adducts or cross-linked products, which is consistent with previous conclusions that singlet oxygen is not involved in the dityrosine cross-linking (*61*). In view of the high reduction potential of the tyrosyl radical−tyrosine couple (0.88 V)(*63*), a strong oxidant or high-energy UV light is required to produce tyrosyl radical, which is believed to be the initial step for dityrosine cross-linking. Neither the singlet oxygen reactive species nor the low-energy light employed in this study is adequate for this purpose.

Additional insight regarding the generation of reactive histidine side chains following the generation of singlet oxygen was obtained from considering CaM in complex with the CaM-binding sequences of target proteins, where light-induced cross-linking is observed between CaM and peptides from MLCK and RyR, and only to a lesser extent for the MLCK* and C28W peptides (Figure 7). Examination of the sequence of all four peptides reveals that both MLCK and RyR contain one histidine; in contrast, MLCK* and C28W do not contain any His residues. There are no other significant differences in the primary sequences, indicating an important role for this His residue in mediating protein cross-linking. In the case of CaM bound to the CaM-binding sequence of MLCK, a high-resolution structure is available (i.e., 1cdl.pdb) (*22*), permitting visual inspection of the relative proximity between the histidine side chains of CaM and MLCK to each other. The side chain of His-107 on CaM is pointed away from the MLCK peptide, with an approximate distance of 15.5 Å from the nearest site on CaM (calculated by Swiss Pdbviewer) (*64*). Given the large distance and steric constraints that block accessibility to the MLCK peptide by the CaM backbone, it is very unlikely that this histidine would contribute to the cross-linking reaction between MLCK and CaM. In contrast, His-9 within the CaM-binding sequence of the MLCK peptide is within contact distance to neighboring side chains in CaM (Figure 7, inset), suggesting that this reactive amino acid, among others, is likely involved in the formation of cross-links that stabilize the complex between CaM and the MLCK peptide.

Conclusions and Future Directions. Fluorophore-assisted light inactivation (FALI) using cell-permeable multiuse affinity probes (e.g., FlAsH) mediates protein inactivation through a singlet oxygen mechanism that functions to oxidize methionine side chains within a protein complex and activates histidine and other side chains as zero-length cross-linkers to stabilize protein associations for subsequent mass spectrometric identification. Understanding this mechanism of action permits a rational choice and design of targeted proteins for FALI and extends its use as a valuable tool in the development of a systems-level understanding of protein−protein interactions that control cell function. For example, FALI will be an important tool in the identification of the function of conserved hypothetical proteins through both the selective inactivation of the protein in question and associated binding partners. Through FALI-induced cross-linking, the identity of binding partners can be established to shed light on both the function of the unknown proteins and their biological pathways.

ACKNOWLEDGMENT

We thank Karen L. Wahl for the use of the MALDI MS and Julie M. Gephart for proofreading. A portion of the research described in this paper was performed in the Environmental Molecular Sciences Laboratory, a national scientific user facility sponsored by DOE's Office of Biological and Environmental Research and located at Pacific Northwest National Laboratory.

SUPPORTING INFORMATION AVAILABLE

Figures showing the deuterium oxide effect on the FALI reaction of calmodulin (Figure 1), azide inhibition of the reaction (Figure 2), and the time courses for the methionine oxidation in the trypsinized peptides (Figure 3). This material is available free of charge via the Internet at http://pubs.acs.org.

REFERENCES

1. Bogdanov, B., and Smith, R. D. (2005) Proteomics by FTICR mass spectrometry: top down and bottom up, *Mass Spectrom. Rev. 24*, 168−200.
2. Collins, F. S., Morgan, M., and Patrinos, A. (2003) The human genome project: lessons from large-scale biology, *Science 300*, 286−290.
3. Frazier, M. E., Johnson, G. M., Thomassen, D. G., Oliver, C. E., and Patrinos, A. (2003) Realizing the potential of the genome revolution: the genomes to life program, *Science 300*, 290−293.
4. Mayer, M. U., Shi, L., and Squier, T. C. (2005) One-step, nondenaturing isolation of an RNA polymerase enzyme complex using an improved multi-affinity probe resin, *Mol. BioSystems 1*, 53−56.
5. Tour, O., Meijer, R. M., Zacharias, D. A., Adams, S. R., and Tsien, R. Y. (2003) Genetically targeted chromophore-assisted light inactivation, *Nat. Biotechnol. 21*, 1505−1508.
6. Jay, D. G. (1988) Selective destruction of protein function by chromophore-assisted laser inactivation, *Proc. Natl. Acad. Sci. U.S.A. 85*, 5454−5458.
7. Beck, S., Sakurai, T., Eustace, B. K., Beste, G., Schier, R., Rudert, F., and Jay, D. G. (2002) Fluorophore-assisted light inactivation: a high-throughput tool for direct target validation of proteins, *Proteomics 2*, 247−255.
8. Marek, K. W., and Davis, G. W. (2002) Transgenically encoded protein photoinactivation (FIAsH−FALI): acute inactivation of synaptotagmin I, *Neuron 36*, 805−813.

9. Surrey, T., Elowitz, M. B., Wolf, P. E., Yang, F., Nedelec, F., Shokat, K., and Leibler, S. (1998) Chromophore-assisted light inactivation and self-organization of microtubules and motors, *Proc. Natl. Acad. Sci. U.S.A. 95*, 4293−4298.
10. Horstkotte, E., Schroder, T., Niewohner, J., Thiel, E., Jay, D. G., and Henning, S. W. (2005) Toward understanding the mechanism of chromophore-assisted laser inactivation—evidence for the primary photochemical steps, *Photochem. Photobiol. 81*, 358−366.
11. Linden, K. G., Liao, J. C., and Jay, D. G. (1992) Spatial specificity of chromophore assisted laser inactivation of protein function, *Biophys. J. 61*, 956−962.
12. Liao, J. C., Roider, J., and Jay, D. G. (1994) Chromophore-assisted laser inactivation of proteins is mediated by the photogeneration of free-radicals, *Proc. Natl. Acad. Sci. U.S.A. 91*, 2659−2663.
13. Stadtman, E. R. (1993) Oxidation of free amino acids and amino acid residues in proteins by radiolysis and by metal-catalyzed reactions, *Annu. Rev. Biochem. 62*, 797−821.
14. Chen, B., Mayer, M. U., Markillie, L. M., Stenoien, D. L., and Squier, T. C. (2005) Dynamic motion of helix A in the amino-terminal domain of calmodulin is stabilized upon calcium activation, *Biochemistry 44*, 905−914.
15. Griffin, B. A., Adams, S. R., and Tsien, R. Y. (1998) Specific covalent labeling of recombinant protein molecules inside live cells, *Science 281*, 269−272.
16. Yap, K. L., Kim, J., Truong, K., Sherman, M., Yuan, T., and Ikura, M. (2000) Calmodulin target database. *J. Struct. Funct. Genomics 1*, 8−14.
17. Babu, Y. S., Bugg, C. E., and Cook, W. J. (1988) Structure of calmodulin refined at 2.2 Å resolution, *J. Mol. Biol. 204*, 191−204.
18. Babu, Y. S., Sack, J. S., Greenhough, T. J., Bugg, C. E., Means, A. R., and Cook, W. J. (1985) Three-dimensional structure of calmodulin, *Nature 315*, 37−40.
19. Chattopadhyaya, R., Meador, W. E., Means, A. R., and Quiocho, F. A. (1992) Calmodulin structure refined at 1.7 Å resolution, *J. Mol. Biol. 228*, 1177−1192.
20. Elshorst, B., Hennig, M., Forsterling, H., Diener, A., Maurer, M., Schulte, P., Schwalbe, H., Griesinger, C., Krebs, J., Schmid, H., Vorherr, T., and Carafoli, E. (1999) NMR solution structure of a complex of calmodulin with a binding peptide of the Ca^{2+} pump, *Biochemistry 38*, 12320−12332.
21. Kuboniwa, H., Tjandra, N., Grzesiek, S., Ren, H., Klee, C. B., and Bax, A. (1995) Solution structure of calcium-free calmodulin, *Nat. Struct. Biol. 2*, 768−776.
22. Meador, W. E., Means, A. R., and Quiocho, F. A. (1992) Target enzyme recognition by calmodulin: 2.4 Å structure of a calmodulin-peptide complex, *Science 257*, 1251−1255.
23. Meador, W. E., Means, A. R., and Quiocho, F. A. (1993) Modulation of calmodulin plasticity in molecular recognition on the basis of x-ray structures, *Science 262*, 1718−1721.
24. Ikura, M., Clore, G. M., Gronenborn, A. M., Zhu, G., Klee, C. B., and Bax, A. (1992) Solution structure of a calmodulin-target peptide complex by multidimensional NMR, *Science 256*, 632−638.
25. Vorherr, T., Quadroni, M., Krebs, J., and Carafoli, E. (1992) Photoaffinity-labeling study of the interaction of calmodulin with the plasma-membrane Ca^{2+} pump, *Biochemistry 31*, 8245−8251.
26. Moore, C. P., Rodney, G., Zhang, J. Z., Santacruz-Toloza, L., Strasburg, G., and Hamilton, S. L. (1999) Apocalmodulin and Ca^{2+} calmodulin bind to the same region on the skeletal muscle Ca^{2+} release channel, *Biochemistry 38*, 8532−8537.
27. Strasburg, G. M., Hogan, M., Birmachu, W., Thomas, D. D., and Louis, C. F. (1988) Site-specific derivatives of wheat-germ calmodulin − interactions with troponin and sarcoplasmic-reticulum, *J. Biol. Chem. 263*, 542−548.
28. Sun, H., Yin, D., Coffeen, L. A., Shea, M. A., and Squier, T. C. (2001) Mutation of Tyr(138) disrupts the structural coupling between the opposing domains in vertebrate calmodulin, *Biochemistry 40*, 9605−9617.
29. Sun, H., Gao, J., Ferrington, D. A., Biesiada, H., Williams, T. D., and Squier, T. C. (1999) Repair of oxidized calmodulin by methionine sulfoxide reductase restores ability to activate the plasma membrane Ca-ATPase, *Biochemistry 38*, 105−112.
30. Tsodikov, O. V., Record, M. T., and Sergeev, Y. V. (2002) Novel computer program for fast exact calculation of accessible and molecular surface areas and average surface curvature, *J. Comput. Chem. 23*, 600−609.
31. Bondi, A. (1964) Van der Waals volumes and radii, *J. Phys. Chem. 68*, 441.
32. Bartlett, R. K., Bieber Urbauer, R. J., Anbanandam, A., Smallwood, H. S., Urbauer, J. L., and Squier, T. C. (2003) Oxidation of Met144 and Met145 in calmodulin blocks calmodulin dependent activation of the plasma membrane Ca-ATPase, *Biochemistry 42*, 3231−3238.
33. Gao, J., Yin, D., Yao, Y., Williams, T. D., and Squier, T. C. (1998) Progressive decline in the ability of calmodulin isolated from aged brain to activate the plasma membrane Ca-ATPase, *Biochemistry 37*, 9536−9548.
34. Ogilby, P. R., and Foote, C. S. (1983) Chemistry of singlet oxygen. 42. Effect of solvent, solvent isotopic-substitution, and temperature on the lifetime of singlet molecular-oxygen ($^1\Delta_g$), *J. Am. Chem. Soc. 105*, 3423−3430.
35. Davies, M. J. (2004) Reactive species formed on proteins exposed to singlet oxygen, *Photochem. Photobiol. Sci. 3*, 17−25.
36. Sharov, V. S., Ferrington, D. A., Squier, T. C., and Schoneich, C. (1999) Diastereoselective reduction of protein-bound methionine sulfoxide by methionine sulfoxide reductase, *FEBS Lett. 455*, 247−250.
37. Sharov, V. S., and Schoneich, C. (2000) Diastereoselective protein methionine oxidation by reactive oxygen species and diastereoselective repair by methionine sulfoxide reductase, *Free Radical Biol. Med. 29*, 986−994.
38. Tomita, M., Irie, M., and Ukita, T. (1969) Sensitized photooxidation of histidine and its derivatives. Products and mechanism of the reaction, *Biochemistry 8*, 5149−5160.
39. Yin, D., Kuczera, K., and Squier, T. C. (2000) The sensitivity of carboxyl-terminal methionines in calmodulin isoforms to oxidation by H_2O_2 modulates the ability to activate the plasma membrane Ca-ATPase, *Chem. Res. Toxicol. 13*, 103−110.
40. Anbanandam, A., Bieber Urbauer, R. J., Bartlett, R. K., Smallwood, H. S., Squier, T. C., and Urbauer, J. L. (2005) Mediating molecular recognition by methionine oxidation: conformational switching by oxidation of methionine in the carboxyl-terminal domain of calmodulin, *Biochemistry 44*, 9486−9496.
41. Chen, B., Mayer, M. U., and Squier, T. C. (2005) Structural uncoupling between opposing domains of oxidized calmodulin underlies the enhanced binding affinity and inhibition of the plasma membrane Ca-ATPase, *Biochemistry 44*, 4737−4747.
42. Widengren, J., Mets, U., and Rigler, R. (1995) Fluorescence correlation spectroscopy of triplet-states in solution: a theoretical and experimental-study, *J. Phys. Chem. 99*, 13368−13379.
43. Gorman, A. A. (1992) The bimolecular reactivity of singlet oxygen, *Adv. Photochem. 17*, 217−275.
44. Ochsner, M. (1997) Photophysical and photobiological processes in the photodynamic therapy of tumours, *J. Photochem. Photobiol., B 39*, 1−18.
45. Huhmer, A. F., Gerber, N. C., Ortiz de Montellano, P. R., and Schoneich, C. (1996) Peroxynitrite reduction of calmodulin stimulation of neuronal nitric oxide synthase, *Chem. Res. Toxicol. 9*, 484−491.
46. Huhmer, A. F., Nishida, C. R., Ortiz de Montellano, P. R., and Schoneich, C. (1997) Inactivation of the inducible nitric oxide synthase by peroxynitrite, *Chem. Res. Toxicol. 10*, 618−626.
47. Shen, H. R., Spikes, J. D., Smith, C. J., and Kopecek, J. (2000) Photodynamic cross-linking of proteins. IV. Nature of the His-His bond(s) formed in the rose bengal-photosensitized cross-linking of *N*-benzoyl-L-histidine, *J. Photochem. Photobiol., A 130*, 1−6.
48. Verweij, H., and Vansteveninck, J. (1982) Model studies on photodynamic cross-linking, *Photochem. Photobiol. 35*, 265−267.
49. Bigelow, D. J., and Squier, T. C. (2005) Redox modulation of cellular signaling and metabolism through reversible oxidation of methionine sensors in calcium regulatory proteins, *Biochim. Biophys. Acta 1703*, 121−34.
50. Gao, J., Yao, Y., and Squier, T. C. (2001) Oxidatively modified calmodulin binds to the plasma membrane Ca-ATPase in a nonproductive and conformationally disordered complex, *Biophys. J. 80*, 1791−1801.
51. Yao, Y., Yin, D., Jas, G. S., Kuczer, K., Williams, T. D., Schoneich, C., and Squier, T. C. (1996) Oxidative modification of a carboxyl-terminal vicinal methionine in calmodulin by hydrogen peroxide inhibits calmodulin-dependent activation of the plasma membrane Ca-ATPase, *Biochemistry 35*, 2767−2787.
52. Black, D. J., Tran, Q. K., and Persechini, A. (2004) Monitoring the total available calmodulin concentration in intact cells over the physiological range in free Ca^{2+}, *Cell Calcium 35*, 415−425.

53. Davies, M. J. (2005) The oxidative environment and protein damage, *Biochim. Biophys. Acta 1703*, 93−109.
54. Persechini, A., and Stemmer, P. M. (2002) Calmodulin is a limiting factor in the cell, *Trends Cardiovasc. Med. 12*, 32−37.
55. Tran, Q. K., Black, D. J., and Persechini, A. (2003) Intracellular coupling via limiting calmodulin, *J. Biol. Chem. 278*, 24247−24250.
56. Gellman, S. H. (1991) On the role of methionine residues in the sequence-independent recognition of nonpolar protein surfaces, *Biochemistry 30*, 6633−6636.
57. Michaeli, A., and Feitelson, J. (1994) Reactivity of singlet oxygen toward amino-acids and peptides, *Photochem. Photobiol. 59*, 284−289.
58. Balog, E. M., Norton, L. E., Bloomquist, R. A., Cornea, R. L., Black, D. J., Louis, C. F., Thomas, D. D., and Fruen, B. R. (2003) Calmodulin oxidation and methionine to glutamine substitutions reveal methionine residues critical for functional interaction with ryanodine receptor-1, *J. Biol. Chem. 278*, 15615−15621.
59. Balog, E. M., Norton, L. E., Thomas, D. D., and Fruen, B. R. (2006) Role of calmodulin methionine residues in mediating the productive association with cardiac ryanodine receptors, *Am. J. Physiol.: Heart Circ. Physiol 290*, H794−H799.
60. Montgomery, H. J., Bartlett, R., Perdicakis, B., Jervis, E., Squier, T. C., and Guillemette, J. G. (2003) Activation of constitutive nitric oxide synthases by oxidized calmodulin mutants, *Biochemistry 42*, 7759−7768.
61. Balasubramanian, D., Du, X., and Zigler, J. S. (1990) The reaction of singlet oxygen with proteins, with special reference to crystallins, *Photochem. Photobiol. 52*, 761−768.
62. Malencik, D. A., and Anderson, S. R. (2003) Dityrosine as a product of oxidative stress and fluorescent probe, *Amino Acids 25*, 233−247.
63. Giulivi, C., and Cadenas, E. (1998) Heme protein radicals: formation, fate, and biological consequences, *Free Radical Biol. Med. 24*, 269−279.
64. Guex, N., and Peitsch, M. C. (1997) SWISS-MODEL and the Swiss-PdbViewer: an environment for comparative protein modeling, *Electrophoresis 18*, 2714−2723.

BI052395A